JACS
JOURNAL OF THE AMERICAN CHEMICAL SOCIETY
Article
pubs.acs.org/JACS

Tumor Acidity-Sensitive Polymeric Vector for Active Targeted siRNA Delivery

Chun-Yang Sun,[†,∥] Song Shen,[†,∥] Cong-Fei Xu,[‡] Hong-Jun Li,[†] Yang Liu,[†] Zhi-Ting Cao,[‡] Xian-Zhu Yang,[†] Jin-Xing Xia,[†] and Jun Wang*[,†,‡,§]

[†]The CAS Key Laboratory of Innate Immunity and Chronic Disease, School of Life Sciences and Medical Center, University of Science & Technology of China, Hefei, Anhui 230027, PR China

[‡]Hefei National Laboratory for Physical Sciences at Microscale, University of Science and Technology of China, Hefei, Anhui 230027, PR China

[§]Innovation Center for Cell Signaling Network, University of Science and Technology of China, Hefei, Anhui 230027, PR China

Supporting Information

ABSTRACT: Although surface PEGylation of siRNA vectors is effective for preventing protein adsorption and thereby helps these vectors to evade the reticuloendothelial system (RES) in vivo, it also suppresses the cellular uptake of these vectors by target cells. This dilemma could be overcome by employing stimuli-responsive shell-detachable nanovectors to achieve enhanced cellular internalization while maintaining prolonged blood circulation. Among the possible stimuli, dysregulated pH in tumor (pH_e) is the most universal and practical. However, the design of pH_e-sensitive system is problematic because of the subtle differences between the pH_e and pH in other tissues. Here, a simple acid-sensitive bridged copolymer is developed and used for tumor-targeted systemic delivery of siRNA. After forming the micelleplex delivery system, the corresponding nanoparticles (D_m-NP) might undergo several modifications as follows: (i) a poly(ethylene glycol) (PEG) corona, which is stable in the circulatory system and protects nanovectors from RES clearance; (ii) a pH_e responsive linkage breakage, which induces PEG detachment at tumor sites and thereby facilitates cell targeting; and (iii) a cell-penetration peptide, which is exposed upon the removal of PEG and further enhances cellular uptake. Thus, D_m-NP achieved both prolonged circulation and effective accumulation in tumor cells and resulted in the safe and enhanced inhibition of non-small cell lung cancer growth.

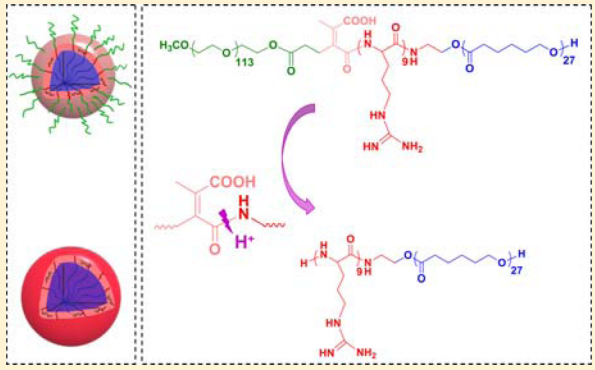

INTRODUCTION

Interest in utilizing biopharmaceutical agents, including specific proteins, nucleic acids and polysaccharides, for cancer therapy has grown rapidly in recent years.[1−3] However, the clinical applications of these agents are hampered by their inability to reach the intended target tissue (e.g., tumors), cross the cell membrane and exert their therapeutic activities.[4−6] Accordingly, PEGylated polymeric delivery systems are highly desirable because they can protect these biomacromolecules from clearance, and subsequently promote their accumulation at tumor sites.[7,8] To date, a key challenge in maximizing the efficacy and application potentials of biopharmaceutical agents is the reduced cellular uptake of PEGylated nanoparticles, which plays a crucial role in stabilizing nanoparticles, minimizing nonspecific protein interactions and reducing clearance by immune cells.[9,10] Although nanoparticles with functional ligand modifications, such as a specific targeting groups and/or highly cationic cell-penetrating peptides (CPP), have been successfully used for the extracellular and intracellular delivery of various cargoes in vitro, they have generally been considered unsuitable for many in vivo studies because of unavoidable nonspecific interactions and recognition in normal tissues.[11,12] For instance, accelerated clearance and deep penetration in most organs have been observed after systemic injection of CPP functional delivery systems.[13]

So far, one of the most common approaches to enhancing cellular internalization is to bury or protect the functional group while it is in the circulatory system, and the shield can then be removed when exposed to specific tumor microenvironment; this process is the so-called "presentation" strategy.[14] For example, Xiang and colleagues added the tripeptide substrate of the endoprotease legumain to the fourth lysine residue in the trans-activating activator (TAT) to decrease the transmembrane transport capacity to 27.35%. Once the nanoparticles accumulate in a tumor, abundant legumain cleaved the protection groups and recovered the penetrating function of the deprotected TAT.[15] In addition, Torchilin's group has

Received: September 11, 2015
Published: November 16, 2015

DOI: 10.1021/jacs.5b09602
J. Am. Chem. Soc. 2015, 137, 15217−15224

Scheme 1. Polymer-Based Nanoparticles and Their Change in Response to Tumor Acidity[a]

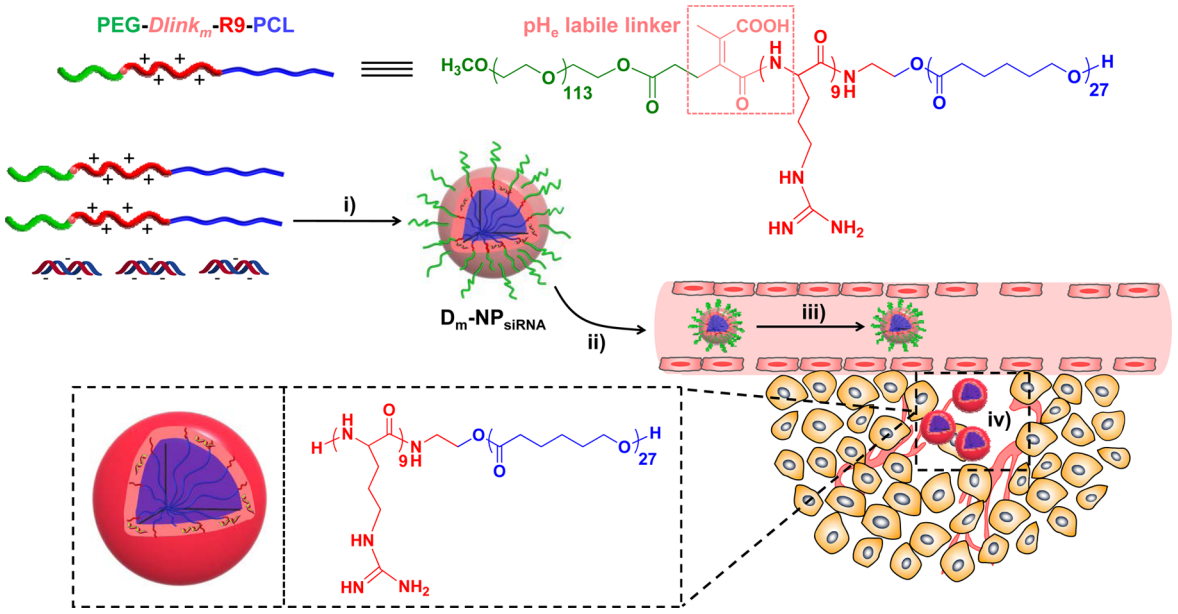

[a](i) Self-assembly of PEG-*Dlink*$_m$-R9-PCL into nanoparticles in aqueous solution and formation of D$_m$-NP$_{siRNA}$ after binding with negatively charged siRNA. (ii) Systemic injection of D$_m$-NP$_{siRNA}$. (iii) Prolonged circulation of D$_m$-NP$_{siRNA}$ with protection of extremely stable PEG layer. (iv) Enhanced recognition of D$_m$-NP$_{siRNA}$ by tumor cells following degradation of the *Dlink*$_m$ labile linkage.

utilized the properties of matrix metalloproteinase 2, which is overexpressed and involved in a variety of cancers at different stages, to construct extracellular stimulated nanocarriers. Thus, the protective PEG could be eliminated to expose the CPP through the cleavage of a designed linker followed by cellular uptake and subsequent events.[16,17] Meanwhile, the Warburg effect-induced extracellular pH (pH$_e$) is a more practical trigger than the tumor-specific enzyme that has a variable absolute concentration in different types of cancer.[18] Compared with the success of designing intracellular pH (pH 5.0−6.0) sensitive system to promote the intracellular cargo release,[19−21] the development of ideal pH$_e$ responsive materials are more arduous[22−24] because of the difficulty in controlling the delicate pH sensitivity of nanoparticles between the normal microenvironment (pH 7.2−7.4) and the tumor matrix (~pH 6.2−6.9).[25] One notable example is the "pop-up" mechanism proposed by Bae and colleagues; this mechanism protonates an imidazole group, which ensures that the TAT or biotin is outspreaded after it accumulates in the tumor.[26,27]

2,3-Dimethylmaleamidic acid (DMMA) has been employed as an excellent candidate for designing acidity-controlled deshielding systems because of its extreme sensitivity to pH$_e$.[28−30] Unfortunately, the quick cleavage kinetics and unsatisfactory stability of the amide bond at pH 7.4 limit its further application.[31] Moreover, DMMA can only be used to modify polymer side groups. It is believed that the methyl group plays a crucial role in the acidic sensitivity of the amide bond in dimethylmaleamidic acid.[32] In addition, introducing another functional group to replace the methyl group of DMMA has been successfully used to provide an additional reaction site and achieve a slower degradation rate.[33−35] Therefore, we propose that expanding the materials toolbox using 2-propionic-3-methylmaleic anhydride (CDM) to fabricate a pH$_e$-facilitated deprotection system is reasonable. To validate our hypothesis, we developed a functional nanomaterial containing a degradable bridged bond (*Dlink*$_m$) that directed pH$_e$-responsive cationic nona-arginine (R9) exposure and tested whether the promoted tumor cell uptake and ultimate tumor cell-targeted siRNA delivery could be achieved (Scheme 1). The effectiveness of this approach for biomacromolecules-based anticancer therapy was evaluated in vitro and in vivo.

RESULTS AND DISCUSSION

Design of *Dlink*$_m$ Bridged Copolymer and the Micelleplex System. Compared with 2,3-dimethylmaleic anhydride, the carboxyl group of CDM offers one additional reaction site to construct a bridged responsive copolymer and decelerate the sensitivity of linkage to pH 7.4, thus satisfying the requirement of cellular uptake.[36,37] First, PEG was modified as PEG-DMA after the well-established synthesis of chlorine-substituted CDM (Figure S1). Successful and complete CDM introduction into the polymer terminal group was confirmed by the ^{1}H NMR spectrum (Figure S2). Then, PEG-DMA was coupled with an amine-functionalized poly(ε-caprolactone)-R9 (PCL-R9), which was obtained via the deprotection of the Fmoc group (characterizations are shown in Figures S3−4). The products after coupling reactions between macromolecules usually include a large number of homopolymers because of inefficient purification.[38] Notably, the PEG-*Dlink*$_m$-R9-PCL profile by gel permeation chromatography (GPC) showed an obvious shift toward higher molecular weight, whereas a homopolymer peak was not observed after the purification of excess PEG-DMA using amino-functionalized resin (Figure S5), which suggests that the resin is a better choice for entirely removing residual homopolymer. Figure S6 indicates that the molar ratio of PCL, R9 and PEG was 1:0.97:1.05, which is close to that of the desired bridged copolymer. Moreover, the peak splitting of methyl protons (1.90−2.05 ppm) in maleamidic acid moiety suggests that the successful cyclic anhydride opening since the targeted copolymer had a mixed sequence of α and β isomers (only α isomers are depicted). To investigate the effect of the pH$_e$ sensitive *Dlink*$_m$ linkage on the

DOI: 10.1021/jacs.5b09602
J. Am. Chem. Soc. 2015, 137, 15217−15224

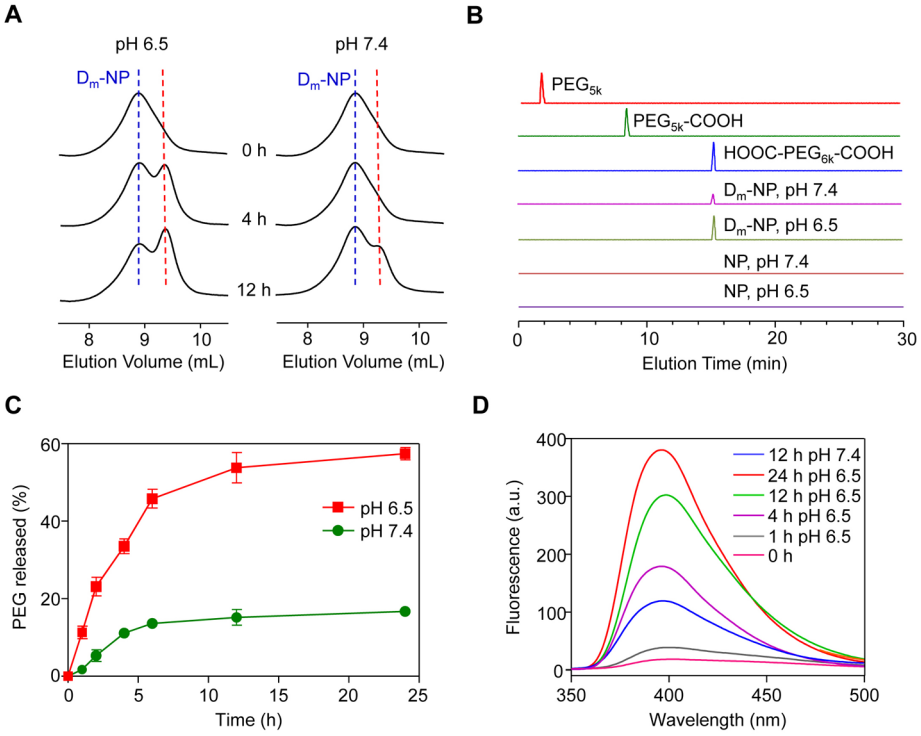

Figure 1. (A) Degradation of D_m-NP incubated at pH 6.5 or 7.4 for different periods of time by GPC analyses. Homopolymers were observed at 9.4 mL (indicated by red dashed line). (B) HPLC analyses of PEG_{5k}, PEG_{5k}-COOH, HOOC-PEG_{6k}-COOH, D_m-NP and NP incubated at pH 6.5 or 7.4. (C) Quantitative analyses of the degradation of D_m-NP incubated at pH 6.5 or 7.4. (D) The fluorescence emission spectra of reaction products between 9,10-phenanthraquinone and D_m-NP, which were preincubated for different periods of time.

nanoparticles, we synthesized nondegradable PEG-R9-PCL as the control through NHS/DIC-catalyzed coupling reaction, whereas PEG-DMA was replaced with PEG-NHS (Figure S7).

Micellar nanoparticles were fabricated through the solvent exchange method using PEG-*Dlink*$_m$-R9-PCL and PEG-R9-PCL. The obtained micelles were denoted as D_m-NP and NP, respectively. The diameter and zeta potential of both nanoparticles measured by transmission electron microscopy and dynamic light scattering, were ∼100 nm and ∼40 mV, respectively (Figure S8), and these values proved to be more suitable for passive tumor targeting via the enhanced permeability and retention (EPR) effect.[39,40]

pH_e Sensitivity of *Dlink*$_m$ Group. Because CDM and its derivatives have been shown to be sensitive to the extracellular microenvironment and used to design acidity-responsive polymers, it was expected that we would observe selective cleavage of amide bonds in the *Dlink*$_m$ linker under slightly acidic conditions. Considering degradation yields two homopolymers with different terminal groups, we investigated acidity-triggered degradation using GPC after incubation at pH 6.5 or 7.4. As shown in Figure 1A, there were increasing homopolymers with a prolonged elution volume (9.4 mL) observed under pH_e conditions, which was consistent with the lower molecular weight of PEG and PCL-R9. In sharp contrast, a weaker shoulder peak at identical elution volume was found only after incubation for 12 h at pH 7.4, indicating slower *Dlink*$_m$ cleavage within the same period of time.

Generally, the lack of quantitative methods for the degradation of bridged responsive copolymers is a remarkable obstacle in this field because this degradation can only be measured via the change of the corresponding nanoparticles.[41,42] We built quantitative analyses for *Dlink*$_m$ degradation based on an anion exchange mechanism. The nanoparticles were centrifuged after incubation and the supernatant was freeze-dried to detect the PEG content using high-performance liquid chromatography (HPLC). As shown in Figure 1B, PEG_{5k}-COOH exhibited its peak at an elution time of 9.5 min and HOOC-PEG_{6k}-COOH exhibited its peak at an elution time at 15.4 min. Furthermore, the incubation of D_m-NP at pH 6.5 for 6 h resulted in significant degradation of *Dlink*$_m$ linkages. An enhanced signal was found at an elution time of 15.4 min compared with the signal after incubation at pH 7.4 (Figure S9), which indicated that a bicarboxyl group was present in the PEG derivate. According to the integrated peak area, the cumulative PEG release results revealed a release of less than 20% of total PEG from D_m-NP when incubated at pH 7.4 for 24 h. Conversely, much more rapid release was observed at pH 6.5, with a nearly 60% of cumulative release under otherwise identical conditions (Figure 1C).

The loss of the PEG corona after on-demand degradation reduces the PEG protection of the R9 layer and micellar core, which were formed after self-assembly. It is believed that the R9 layer could be exposed after decreasing PEGylation, which is followed by additional opportunities to contact external structures, such as proteins on cell membranes.[16,43] To confirm this hypothesis, we used the agent 9, 10-phenanthraquinone, which fluoresces after reaction with the guanidine group of arginine,[44] to determine the status of the R9 layer after incubation of D_m-NP at pH 6.5 for different periods of time. The emission spectra of the reaction products (Figure 1D) showed an elevation in guanidine activity because of the correlation of the dramatically increased fluorescence intensity with the prolonged incubation time at pH 6.5, indicating continual R9 layer exposure. However, the NP without the

DOI: 10.1021/jacs.5b09602
J. Am. Chem. Soc. 2015, 137, 15217−15224

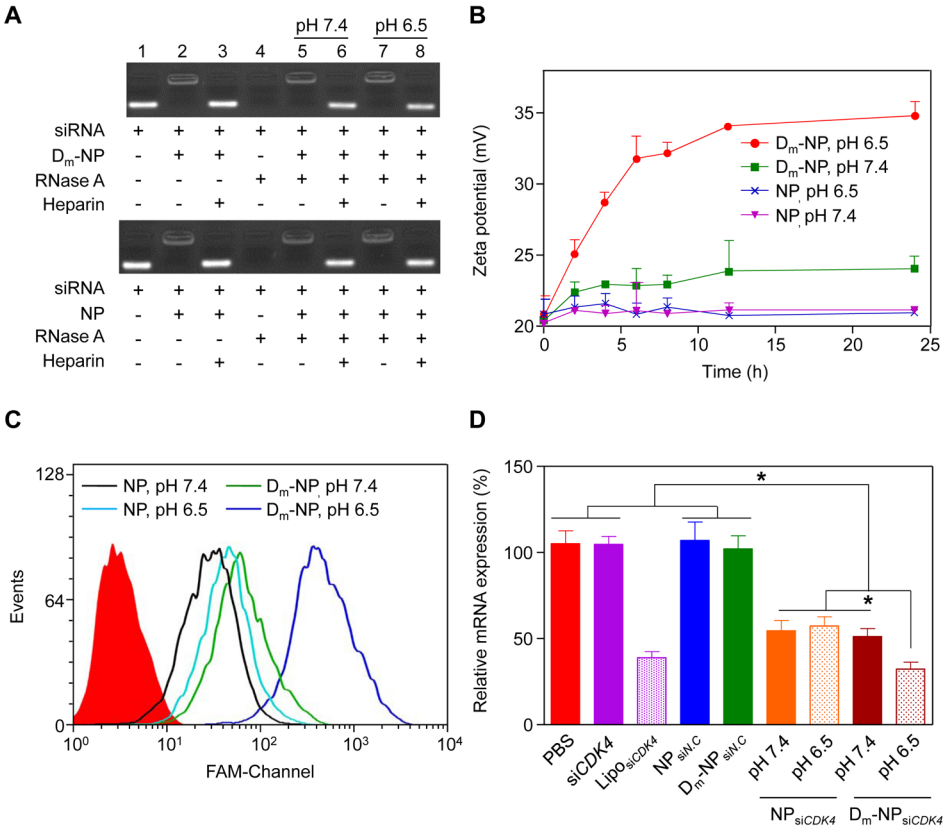

Figure 2. (A) Gel retardation assay of nanoparticles with the indicated treatments and an N/P ratio of 10. Lanes 5 and 7 represent the products treated at pH 7.4, whereas lanes 6 and 8 represent those treated at pH 6.5. (B) Zeta potential of si*N.C.*-loaded NP and D_m-NP after incubation in phosphate buffer (pH 7.4 or 6.5) for 24 h. (C) Flow cytometry analysis of A549 cells after incubation with FAM-siRNA loaded NP or D_m-NP at pH 7.4 or 6.5 for 2 h. The dose of FAM-siRNA was 200 nM in the cell culture. (D) Levels of CDK4 mRNA in KRAS mutant A549 cells after incubation with NP_{siCDK4} or D_m-NP_{siCDK4}. *$p < 0.05$.

degradable linkage bond did not show any degradation, even when incubated at pH 6.5 for the same period of time as in the above-mentioned assays (Figures S10−11). These data demonstrate that the *Dlink*$_m$ linkage group can be specifically cleaved at a slightly lower pH value.

After self-assembly, the R9 in the hydrophilic shell of D_m-NP and NP allows them to bind with siRNA to form micelleplexes. Complete binding of siRNA with both nanoparticles was found at an N/P ratio of 10:1. Moreover, ~85% of the intact siRNA (calculated by ImageJ software) was detected when the nanoparticles were treated by Rnase A and heparin in turn (lanes 6 and 8), suggesting that siRNA could be protected from enzymolysis after RNase A treatment by PEGylated D_m-NP and NP (Figure 2A). In addition, FAM-labeled siRNA was used to examine the siRNA release rate. As shown in Figure S12, following the burst release in the first 8 h, siRNA was sustainably released from NP under both pH conditions. After 168 h of incubation in phosphate buffer, the released siRNA from the nondegradable NP reached nearly 50%. The initial burst release mainly resulted from the diffusion of siRNA bound on or near the surfaces of nanoparticles, which is consistent with the results of previous studies.[45,46] However, the siRNA release in D_m-NP was accelerated at pH 6.5. This PEG detachment-induced rapid siRNA release was also observed in a previous study.[47]

After removal of the PEG shell at pH 6.5, it is believed that the exposed R9 without bound siRNA contribute to the stronger positive surface charge of micelleplexes, which results in promoted cellular internalization.[48,49] We then incubated the nanoparticles at pH 6.5 and monitored the change in surface potential over time. As indicated in Figure 2B, the zeta potential of D_m-$NP_{siN.C.}$ at pH 6.5 significantly increased compared with that at pH 7.4 (approximately 34.8 mV vs 23.9 mV). Conversely, $NP_{siN.C.}$ maintained the original zeta potential at both pH levels. The unchanged surface charge implies that slight acidity only triggers the decomposition of the *Dlink*$_m$ group, which leads to PEG elimination, R9 exposure and subsequent increased positive surface charge.

Extracellular pH Triggered Cellular Uptake and Gene Silencing Analysis. Because the covered PEG corona could be removed at pH 6.5, we next determined the potential of D_m-NP to promote its cellular uptake and thereby increase siRNA accumulation in cells at pH 6.5. A549 cells, a non-small cell lung cancer cell line, were incubated with D_m-$NP_{FAM\text{-}siRNA}$ or $NP_{FAM\text{-}siRNA}$ at pH 6.5 or 7.4 for 2 h, and the intracellular fluorescence intensity was detected by flow cytometry. As shown in Figure 2C, the cellular uptake of D_m-$NP_{FAM\text{-}siRNA}$ at pH 7.4 was very similar to that of $NP_{FAM\text{-}siRNA}$ at both pH levels, indicating that nondegraded PEG chains covering D_m-$NP_{FAM\text{-}siRNA}$ constantly hinder the nanoparticle interactions with cells.[50] However, once the D_m-$NP_{FAM\text{-}siRNA}$ micelles were incubated with A549 cells at pH 6.5, much more efficient cellular uptake of the nanoparticles was observed, suggesting that PEG was readily cleared from the outer layer of the micelle. In addition, the increased internalization of D_m-$NP_{FAM\text{-}siRNA}$ micelles was visualized by confocal microscopy

DOI: 10.1021/jacs.5b09602
J. Am. Chem. Soc. 2015, 137, 15217−15224

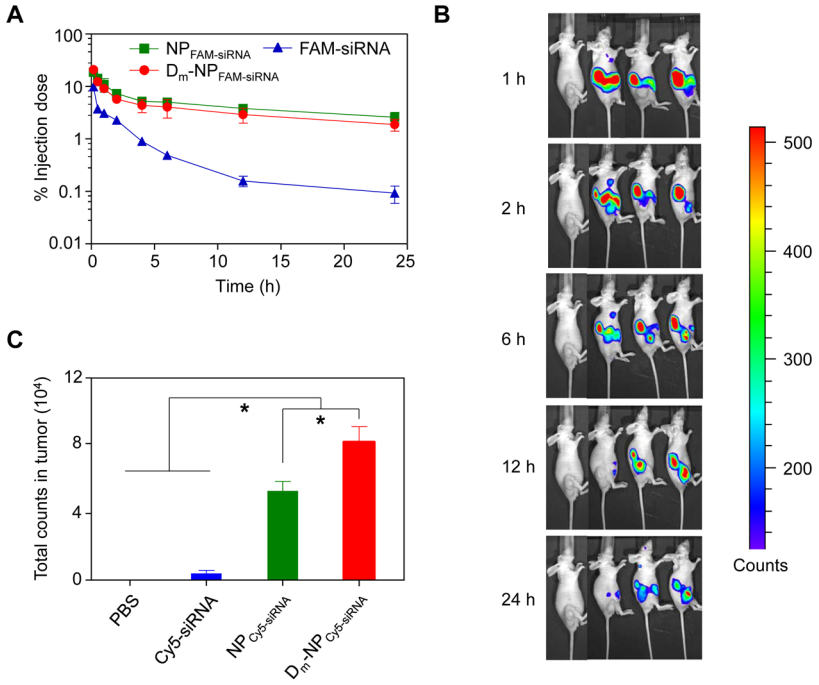

Figure 3. (A) Pharmacokinetics of free FAM-siRNA or FAM-siRNA loaded nanoparticles after i.v. administration (mean ± SD, n = 4). (B) Distribution and tumor accumulation of Cy5-siRNA in A549 tumor-bearing mice receiving intravenous injection of the indicated formulations. The dose of Cy5-siRNA was 1 mg per kg mouse body weight. From left to right are the mice treated with phosphate-buffered saline (PBS), Cy5-siRNA, $NP_{Cy5\text{-}siRNA}$ or $D_m\text{-}NP_{Cy5\text{-}siRNA}$. (C) Cy5-siRNA fluorescence intensity in tumor tissues collected at 24 h following systemic injection. *$p < 0.05$.

(Figure S13). The FAM-siRNA signal was partially detected as a punctate pattern that was not only colocalized with lysosomes and endosomes stained with LysoTracker but also distributed in the cytoplasm where siRNA functions. Because of the acidic microenvironment of the solid tumor interstitial space (~pH 6.2−6.9), it is reasonable to consider that the effective entry into cells and siRNA release into the cytoplasm of $D_m\text{-}NP_{siRNA}$ was subsequently accompanied by enhanced gene silencing. We chose the CDK4 gene in KRAS mutant A549 cells as a target for silencing because of its superior efficacy and selectivity, which was demonstrated by our previous study.[51] Consistent findings were obtained in the siRNA functional experiment at the cellular level. Down-regulation of CDK4 mRNA and protein in a pH-dependent manner was observed in the $D_m\text{-}NP_{siCDK4}$ group, and it was more effective at pH 6.5 than at pH 7.4 (Figures 2D and S14). Notably, significant differences in gene silencing were not observed between pH 7.4 and pH 6.5 when the A549 cells were treated with NP_{siCDK4}. It is well documented that lower expression of CDK4 is associated with the inhibition of KRAS mutant cell proliferation.[52] As shown in Figure S15, knockdown of CDK4 by $D_m\text{-}NP_{siCDK4}$ at pH 6.5 decreased the viability of A549 cells to 22.7 ± 2.1% at a si*CDK4* concentration of 200 nM. A similar trend was shown in a clonogenic assay (Figure S16), whereas the lowest clonogenicity was observed in cells incubated with $D_m\text{-}NP_{siCDK4}$ at pH 6.5.

Pharmacokinetics and Biodistribution in Vivo. When modified with a nondegraded or permanently PEGylated corona, D_m-NP and NP are expected to have prolonged circulation in blood. We analyzed the pharmacokinetics of $D_m\text{-}NP_{FAM\text{-}siRNA}$ and $NP_{FAM\text{-}siRNA}$ in ICR mice. Figure 3A shows the concentration of injected FAM treated with RNase A in plasma versus time after the intravenous administration of $D_m\text{-}NP_{FAM\text{-}siRNA}$, $NP_{FAM\text{-}siRNA}$ or FAM-siRNA. Consistent with previous reports,[53] the *i.v.*-injected free siRNA was rapidly cleared from the bloodstream. However, with PEGylation, both nanoparticles exhibited prolonged circulation in the blood relative to free siRNA. A statistical analysis showed that the area under the curve (AUC) of both PEGylated nanoparticles was significantly increased and 4.24- and 4.15-fold greater than that of free siRNA (AUC_{0-t} 3999.3 nmol h/L). In addition, both nanoparticles extended the terminal half-life ($t_{1/2z}$) of siRNA to nearly 12 h. Thus, it can be concluded that the prolonged circulation behavior of D_m-NP is comparable to that of NP, although the clearance of D_m-NP was accelerated after 12 h, which was likely because of a small amount of PEG degraded at pH 7.4. The pharmacokinetic profiles demonstrated that the PEG corona of D_m-NP was extremely stable in the circulation and reduced the nonspecific interactions between D_m-NP and blood components.

With prolonged blood circulation, nanoparticles have a greater opportunity to accumulate in tumor tissues through the EPR effect.[54,55] We then evaluated the biodistribution of $D_m\text{-}NP_{Cy5\text{-}siRNA}$ and $NP_{Cy5\text{-}siRNA}$ in nude mice bearing A549 lung cancer xenografts (tumor pH ~ 6.5)[22] via fluorescence imaging. Following systemic injection, fluorescent images of mice were acquired at different time intervals. As depicted in Figure 3B, both $D_m\text{-}NP_{Cy5\text{-}siRNA}$ and $NP_{Cy5\text{-}siRNA}$ were captured by the liver and kidney, indicating the nanosized siRNA delivery systems would be cleared and dissociated by kupffer cells and anionic heparan sulfate.[56,57] More importantly, a much higher fluorescent signal was visualized at tumor sites in the $D_m\text{-}NP_{Cy5\text{-}siRNA}$ group compared with the mice administrated $NP_{Cy5\text{-}siRNA}$. The intensity of the signal did not decay from 6 to 24 h, indicating that the nanoparticles assembled by the $Dlink_m$ bridged copolymer accumulated better in tumors. After 24 h, the mice were sacrificed and the total fluorescence counts in tumor tissues from each group were collected (Figure 3C

DOI: 10.1021/jacs.5b09602
J. Am. Chem. Soc. 2015, 137, 15217−15224

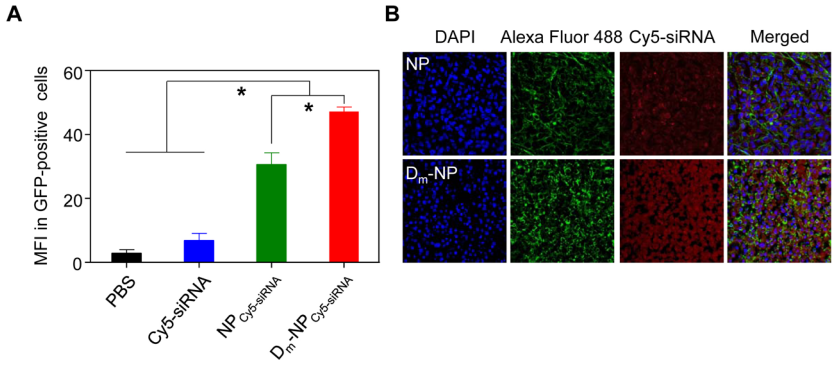

Figure 4. (A) Relative mean fluorescence intensity (MFI) of Cy5-siRNA in GFP-expressing A549 cells analyzed by flow cytometry 24 h after administration (mean ± SD, $n = 4$). (B) A549 tumor cell uptake of Cy5-siRNA loaded nanoparticles observed by confocal microscope. DAPI (blue) and Alexa Fluor 488 phalloidin (green) were used to stain cell nucleus and cytoskeleton, respectively. *$p < 0.05$.

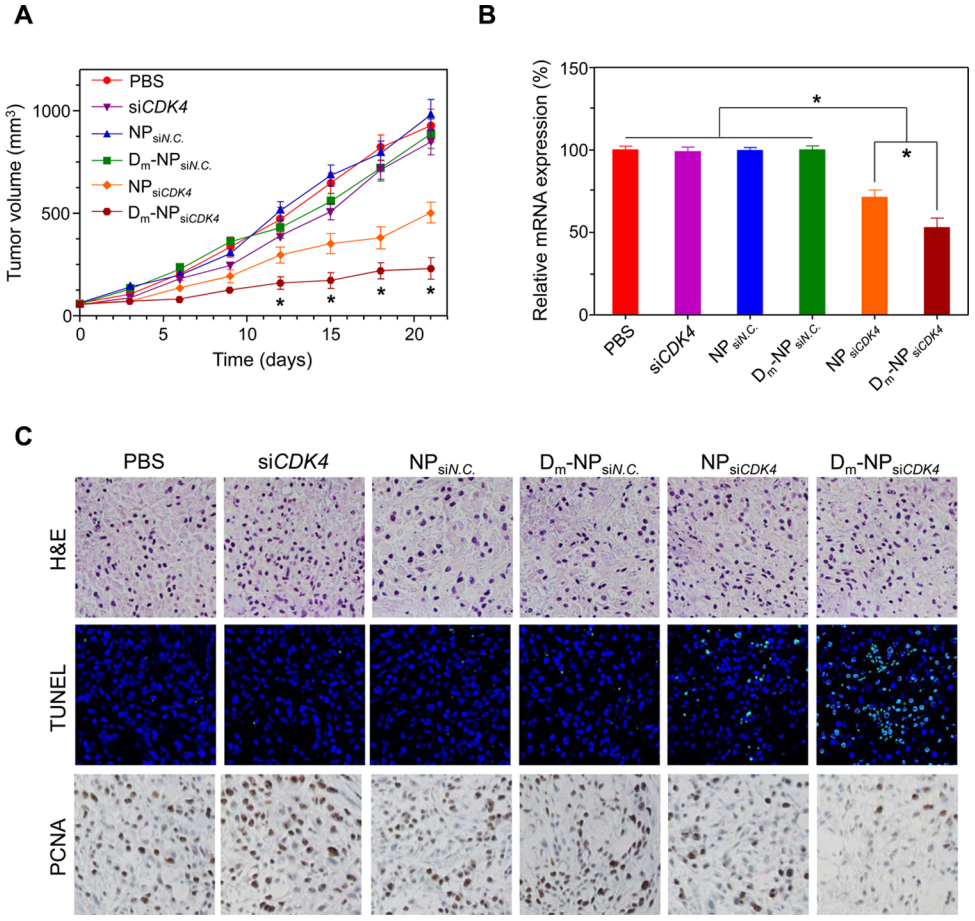

Figure 5. (A) Tumor growth inhibition in A549 tumor xenograft-bearing nude mice after different treatments ($n = 5$). The dose of siRNA was 40 μg per mouse per injection, *$p < 0.05$ when compared with NP_{siCDK4}. (B) Expression of CDK4 mRNA in tumors analyzed at day 22. (C) H&E, TUNEL and PCNA analyses of tumor tissues from mice treated with the indicated formulations. TUNEL-positive apoptotic cells are stained green, and PCNA-positive proliferating cells are stained brown.

and S17). A similar phenomenon considered the strongest Cy5-siRNA fluorescence was detected in the tumor tissues harvested from D_m-$NP_{Cy5\text{-}siRNA}$-treated mice, whereas the $NP_{Cy5\text{-}siRNA}$-treated group showed relatively less fluorescence.

Considering the comparable size, zeta potential and pharmacokinetics of D_m-$NP_{Cy5\text{-}siRNA}$ and $NP_{Cy5\text{-}siRNA}$, the increased tumor accumulation of D_m-$NP_{Cy5\text{-}siRNA}$ could be attributed to the tumor acidity-triggered PEG degradation, which in turn exposes the R9 layer and subsequently promotes the internalization into tumor cells. Even if the $NP_{Cy5\text{-}siRNA}$ could enter the extracellular space of tumor tissue at a comparable rate, PEGylation would hinder its cellular uptake and result in its continual elimination from the tumor site by the lymphatic system and decreased tumor accumulation.[23] To further confirm this hypothesis, we investigated the uptake of nanoparticles in tumor cells in vivo using A549 cells stably expressing green fluorescent protein (GFP). After the injection of Cy5-siRNA loaded nanoparticles, GFP-positive A549 cells were isolated for the analysis of intracellular Cy5 fluorescence intensity by flow cytometry. As shown in Figure 4A, the

DOI: 10.1021/jacs.5b09602
J. Am. Chem. Soc. 2015, 137, 15217−15224

elevated Cy5-siRNA signal was observed in A549-GFP cells when the mice were treated with D_m-$NP_{Cy5\text{-}siRNA}$. In addition, greater cellular uptake of D_m-$NP_{Cy5\text{-}siRNA}$ in A549 cells was also demonstrated in the tumor tissues by using confocal microscopy (Figure 4B). Together, these results show that cleavage of the *Dlink*$_m$ group in D_m-NP, which was stimulated by the tumor pH, substantially attenuated the PEGylation-mediated impediment to cellular internalization and eventually facilitated siRNA accumulation in tumor cells.

Tumor Growth Inhibition of D_m-NP. Finally, the question arose as to whether D_m-NP_{siCDK4} can enhance the silencing efficiency of si*CDK4* in vivo since it appears to promote si*CDK4* internalization after accumulation in the tumor. Thus, we generated A549 tumor xenografts in nude mice and assessed tumor growth following the intravenous administration of different formulations. As illustrated in Figure 5A and S18, tumor inhibition was not observed in mice receiving free si*CDK4*, $NP_{siN.C.}$ or D_m-$NP_{siN.C.}$. However, the growth rate of the tumors in mice receiving NP_{siCDK4} or D_m-NP_{siCDK4} decreased gradually. Of note, D_m-NP_{siCDK4} led to the most pronounced inhibition of tumor growth. Importantly, we found that tumors from mice receiving D_m-NP_{siCDK4} exhibited the most significant down-regulation of CDK4 mRNA and protein expression in tumors following treatment, which suggested a relationship between the inhibition of tumor growth and gene silencing (Figure 5B and S19). However, the CDK4 mRNA levels remained unchanged in tumors from mice treated with phosphate-buffered saline (PBS), free si*CDK4*, $NP_{siN.C.}$ or D_m-$NP_{siN.C.}$. Immunohistochemical studies were highly supportive of the tumor inhibition results described above (Figure 5C). As expected, treatment with D_m-NP_{siCDK4} resulted in significantly reduced proliferation and increased apoptosis compared that of the other groups. In addition, systemic administration of D_m-NP_{siCDK4} in mice had no effect on body weight, liver damage index or innate immune response-related cytokines (Figures S20−21). These data confirm that D_m-NP can significantly enhance the delivery of si*CDK4* to A549 tumor cells with the help of an acidic tumor microenvironment.

CONCLUSIONS

We have successfully engineered a functional nanomaterial with the potential for siRNA delivery using a functionalized maleic anhydride. As a result of the precise introduction of the *Dlink*$_m$ group, the surface function of D_m-NP was altered to enable a response to pH_e. The experiments showed clear evidence that D_m-NP could overcome conflicting PEGylation design to achieve simultaneous prolonged blood circulation after systemic administration and CPP-facilitated cellular uptake in tumor tissues. Systemic administration of D_m-NP exhibited superior gene silencing efficiency and tumor inhibition activity with fewer side effects. Furthermore, compared with previous enzyme-triggered PEG deshielding work, the application of pH_e-responsive D_m-NP is more extensive and practical. This study lays the foundation for further development of such strategies for drug/gene delivery against a wide range of solid tumors.

ASSOCIATED CONTENT

Supporting Information

The Supporting Information is available free of charge on the ACS Publications website at DOI: 10.1021/jacs.5b09602.

Experimental procedures, characterization of *Dlink*$_m$ bridged amphiphilic copolymer, and in vitro and in vivo analysis of the nanocarriers (PDF)

AUTHOR INFORMATION

Corresponding Author

*jwang699@ustc.edu.cn

Author Contributions

‖C.-Y.S. and S.S. contributed equally.

Notes

The authors declare no competing financial interest.

ACKNOWLEDGMENTS

This work was supported by the National Basic Research Program of China (2013CB933900, 2015CB932100, and 2012CB932500), the National Natural Science Foundation of China (51125012, 51390482), and the National High Technology Research and Development Program of China (2014AA020708). The authors thank Prof. Li-Feng Yan and Mr. Li-Yi Fu for the help of GPC analysis.

REFERENCES

(1) Alvarez-Erviti, L.; Seow, Y. Q.; Yin, H. F.; Betts, C.; Lakhal, S.; Wood, M. J. A. *Nat. Biotechnol.* **2011**, *29*, 341.

(2) Sun, Q.; Kang, Z. S.; Xue, L. J.; Yin, Q.; Shang, Y. K.; Su, Z. G.; Sun, H. B.; Ping, Q. N.; Mo, R.; Zhang, C. *J. Am. Chem. Soc.* **2015**, *137*, 6000.

(3) Whitehead, K. A.; Langer, R.; Anderson, D. G. *Nat. Rev. Drug Discovery* **2009**, *8*, 129.

(4) Sun, W. J.; Jiang, T. Y.; Lu, Y.; Reiff, M.; Mo, R.; Gu, Z. *J. Am. Chem. Soc.* **2014**, *136*, 14722.

(5) Kanasty, R.; Dorkin, J. R.; Vegas, A.; Anderson, D. *Nat. Mater.* **2013**, *12*, 967.

(6) Ozcan, G.; Ozpolat, B.; Coleman, R. L.; Sood, A. K.; Lopez-Berestein, G. *Adv. Drug Delivery Rev.* **2015**, *87*, 108.

(7) Davis, M. E.; Zuckerman, J. E.; Choi, J. H. J.; Seligson, D.; Tolcher, A.; Alabi, C. A.; Yen, Y.; Heidel, J. D.; Ribas, A. *Nature* **2010**, *464*, 1067.

(8) Li, J. G.; Yu, X. S.; Wang, Y.; Yuan, Y. Y.; Xiao, H.; Cheng, D.; Shuai, X. T. *Adv. Mater.* **2014**, *26*, 8217.

(9) Knop, K.; Hoogenboom, R.; Fischer, D.; Schuber, U. S. *Angew. Chem., Int. Ed. Engl.* **2010**, *49*, 6299.

(10) Graf, N.; Bielenberg, D. R.; Kolishetti, N.; Muus, C.; Banyard, J.; Farokhzad, O. C.; Lippard, S. J. *ACS Nano* **2012**, *6*, 4530.

(11) Yin, L. C.; Song, Z. Y.; Kim, K. H.; Zheng, N.; Gabrielson, N. P.; Cheng, J. J. *Adv. Mater.* **2013**, *25*, 3063.

(12) Drin, G.; Cottin, S.; Blanc, E.; Rees, A. R.; Temsamani, J. *J. Biol. Chem.* **2003**, *278*, 31192.

(13) Sarko, D.; Beijer, B.; Boy, R. G.; Nothelfer, E. M.; Leotta, K.; Eisenhut, M.; Altmann, A.; Haberkorn, U.; Mier, W. *Mol. Pharmaceutics* **2010**, *7*, 2224.

(14) Ge, Z. S.; Liu, S. Y. *Chem. Soc. Rev.* **2013**, *42*, 7289.

(15) Liu, Z.; Xiong, M.; Gong, J.; Zhang, Y.; Bai, N.; Luo, Y.; Li, L.; Wei, Y.; Liu, Y.; Tan, X.; Xiang, R. *Nat. Commun.* **2014**, *5*, 4280.

(16) Zhu, L.; Wang, T.; Perche, F.; Taigind, A.; Torchilin, V. P. *Proc. Natl. Acad. Sci. U. S. A.* **2013**, *110*, 17047.

(17) Zhu, L.; Kate, P.; Torchilin, V. P. *ACS Nano* **2012**, *6*, 3491.

(18) Alfarouk, K. O.; Muddathir, A. K.; Shayoub, M. E. A. *Cancers* **2011**, *3*, 408.

(19) Lee, C. C.; MacKay, J. A.; Frechet, J. M.; Szoka, F. C. *Nat. Biotechnol.* **2005**, *23*, 1517.

(20) Lee, C. C.; Gillies, E. R.; Fox, M. E.; Guillaudeu, S. J.; Frechet, J. M.; Dy, E. E.; Szoka, F. C. *Proc. Natl. Acad. Sci. U. S. A.* **2006**, *103*, 16649.

(21) Gao, W. W.; Chan, J. M.; Farokhzad, O. *Mol. Pharmaceutics* **2010**, *7*, 1913.

DOI: 10.1021/jacs.5b09602
J. Am. Chem. Soc. 2015, 137, 15217−15224

(22) Wang, Y. G.; Zhou, K. J.; Huang, G.; Hensley, C.; Huang, X. N.; Ma, X. P.; Zhao, T.; Sumer, D. B.; DeBerardinis, J. R.; Gao, J. M. *Nat. Mater.* **2014**, *13*, 204.
(23) Jin, E. L.; Zhang, B.; Sun, X. R.; Zhou, Z. X.; Ma, X. P.; Sun, Q. H.; Tang, J. B.; Shen, Y. Q.; Van Kirk, E.; Murdoch, W. J.; Radosz, M. *J. Am. Chem. Soc.* **2013**, *135*, 933.
(24) Mizuhara, T.; Saha, K.; Moyano, D. F.; Kim, C. S.; Yan, B.; Kim, Y. K.; Rotello, V. M. *Angew. Chem., Int. Ed.* **2015**, *54*, 6567.
(25) Cardone, R. A.; Casavola, V.; Reshkin, S. J. *Nat. Rev. Cancer* **2005**, *5*, 786.
(26) Lee, E. S.; Gao, Z.; Kim, D.; Park, K.; Kwon, I. C.; Bae, Y. H. *J. Controlled Release* **2008**, *129*, 228.
(27) Lee, E. S.; Na, K.; Bae, Y. H. *Nano Lett.* **2005**, *5*, 325.
(28) Du, J. Z.; Du, X. J.; Mao, C. Q.; Wang, J. *J. Am. Chem. Soc.* **2011**, *133*, 17560.
(29) Yang, X. Z.; Du, X. J.; Liu, Y.; Zhu, Y. H.; Liu, Y. Z.; Li, Y. P.; Wang, J. *Adv. Mater.* **2014**, *26*, 931.
(30) Wang, C.; Cheng, L.; Liu, Y.; Wang, X.; Ma, X.; Deng, Z.; Li, Y.; Liu, Z. *Adv. Funct. Mater.* **2013**, *23*, 3077.
(31) Du, J. Z.; Mao, C. Q.; Yuan, Y. Y.; Yang, X. Z.; Wang, J. *Biotechnol. Adv.* **2014**, *32*, 789.
(32) Kang, S.; Kim, Y.; Song, Y.; Choi, J. U.; Park, E.; Choi, W.; Park, J.; Lee, Y. *Bioorg. Med. Chem. Lett.* **2014**, *24*, 2364.
(33) Guo, S.; Huang, Y.; Jiang, Q.; Sun, Y.; Deng, L.; Liang, Z.; Du, Q.; Xing, J.; Zhao, Y.; Wang, P. C.; Dong, A.; Liang, X. J. *ACS Nano* **2010**, *4*, 5505.
(34) Maier, K.; Wagner, E. *J. Am. Chem. Soc.* **2012**, *134*, 10169.
(35) Takemoto, H.; Miyata, K.; Hattori, S.; Ishii, T.; Suma, T.; Uchida, S.; Nobuhiro, N.; Kataoka, K. *Angew. Chem., Int. Ed.* **2013**, *52*, 6218.
(36) Hatakeyama, H.; Akita, H.; Harashima, H. *Adv. Drug Delivery Rev.* **2011**, *63*, 152.
(37) Hatakeyama, H.; Akita, H.; Kogure, K.; Oishi, M.; Nagasaki, Y.; Kihira, Y.; Ueno, M.; Kobayashi, H.; Kikuchi, H.; Harashima, H. *Gene Ther.* **2007**, *14*, 68.
(38) Gao, H. F.; Matyjaszewski, K. *J. Am. Chem. Soc.* **2007**, *129*, 6633.
(39) Maeda, H.; Wu, J.; Sawa, T.; Matsumura, Y.; Hori, K. *J. Controlled Release* **2000**, *65*, 271.
(40) Liang, S.; Yang, X. Z.; Du, X. J.; Wang, H. J.; Li, H. J.; Liu, W. W.; Yao, Y. Y.; Zhu, Y. H.; Ma, Y. C.; Wang, J.; Song, E. W. *Adv. Funct. Mater.* **2015**, *25*, 4778.
(41) Tang, L. Y.; Wang, Y. C.; Li, Y.; Du, J. Z.; Wang, J. *Bioconjugate Chem.* **2009**, *20*, 1095.
(42) Ma, N.; Li, Y.; Xu, H. P.; Wang, Z.; Zhang, X. *J. Am. Chem. Soc.* **2010**, *132*, 442.
(43) Veiman, K.-L.; Künnapuu, K.; Lehto, T.; Kiisholts, K.; Pärn, K.; Langel, Ü.; Kurrikoff, K. *J. Controlled Release* **2015**, *209*, 238.
(44) Smith, R. E.; Macquarrie, R. *Anal. Biochem.* **1978**, *90*, 246.
(45) Xu, X. Y.; Xie, K.; Zhang, X. Q.; Pridgen, E. M.; Park, G. Y.; Cui, D. S.; Shi, J. J.; Wu, J.; Kantoff, P. W.; Lippard, S. J.; Langer, R.; Walker, G. C.; Farokhzad, O. C. *Proc. Natl. Acad. Sci. U. S. A.* **2013**, *110*, 18638.
(46) Chen, Y. H.; Xu, G.; Zheng, Y.; Yan, M. S.; Li, Z. H.; Zhou, Y. Y.; Mei, L.; Li, X. M. *Int. J. Nanomed.* **2015**, *10*, 1375.
(47) Xu, M. H.; Qian, J. M.; Suo, A. L.; Cui, N.; Yao, Y.; Xu, W. J.; Liu, T.; Wang, H. J. *J. Mater. Chem. B* **2015**, *3*, 2215.
(48) Romberg, B.; Hennink, W. E.; Storm, G. *Pharm. Res.* **2008**, *25*, 55.
(49) Maeda, T.; Fujimoto, K. *Colloids Surf., B* **2006**, *49*, 15.
(50) Gref, R.; Luck, M.; Quellec, P.; Marchand, M.; Dellacherie, E.; Harnisch, S.; Blunk, T.; Muller, R. H. *Colloids Surf., B* **2000**, *18*, 301.
(51) Mao, C. Q.; Xiong, M. H.; Liu, Y.; Shen, S.; Du, X. J.; Yang, X. Z.; Dou, S.; Zhang, P. Z.; Wang, J. *Mol. Ther.* **2014**, *22*, 964.
(52) Scholl, C.; Frohling, S.; Dunn, I. F.; Schinzel, A. C.; Barbie, D. A.; Kim, S. Y.; Silver, S. J.; Tamayo, P.; Wadlow, R. C.; Ramaswamy, S.; Dohner, K.; Bullinger, L.; Sandy, P.; Boehm, J. S.; Root, D. E.; Jacks, T.; Hahn, W. C.; Gilliland, D. G. *Cell* **2009**, *137*, 821.
(53) Schroeder, A.; Levins, C. G.; Cortez, C.; Langer, R.; Anderson, D. G. *J. Intern. Med.* **2010**, *267*, 9.
(54) Weissleder, R.; Tung, C. H.; Mahmood, U.; Bogdanov, A. *Nat. Biotechnol.* **1999**, *17*, 375.
(55) Robinson, J. T.; Hong, G. S.; Liang, Y. Y.; Zhang, B.; Yaghi, O. K.; Dai, H. J. *J. Am. Chem. Soc.* **2012**, *134*, 10664.
(56) Zuckerman, J. E.; Choi, C. H. J.; Han, H.; Davis, M. E. *Proc. Natl. Acad. Sci. U. S. A.* **2012**, *109*, 3137.
(57) Petros, R. A.; Desimone, J. M. *Nat. Rev. Drug Discovery* **2010**, *9*, 615.

DOI: 10.1021/jacs.5b09602
J. Am. Chem. Soc. 2015, 137, 15217−15224